Structured Light Scanning of Skin, Muscle and Fat

Wilm, Jakob; Jensen, Sebastian Hoppe Nesgaard; Aanæs, Henrik

Publication date:
2015

Document Version
Publisher's PDF, also known as Version of record

DTU Compute Technical Report-2015-07

Structured Light Scanning of Skin, Muscle and Fat

Jakob Wilm, Sebastian Nesgaard Jensen, and Henrik Aanæs

Department of Applied Mathematics and Computer Science
Technical University of Denmark

Abstract

We investigate the quality of structured light 3D scanning on pig skin, muscle and fat. These particular materials are interesting in a number of industrial and medical use-cases, and somewhat challenging because they exhibit subsurface light scattering. Our goal therefor is to quantify the amount of error that various encoding strategies show, and propose an error correcting model, which can bring down the measurement bias considerably. Samples of raw and unprocessed pig tissue were used with the number of sampled surface points $N_{\text{meat}} = 1.2 \cdot 10^6$, $N_{\text{skin}} = 4.0 \cdot 10^6$ and $N_{\text{fat}} = 2.1 \cdot 10^6$ from 8 different pieces of tissue. With the standard N-step phase shifting method, the bias and RMS errors were found to be 0.45 ± 0.22 mm (muscle), 0.51 ± 0.19 mm (skin) and 0.14 ± 0.16 mm (fat). After applying a linear correction model containing view, light angles and point distances, the bias was almost completely removed on test data, and standard deviations slightly reduced. To our knowledge this is the first quantitative study of the measurement error of structured light with biological tissue.

1 Introduction

Structured light has become a very popular and versatile method for 3D acquisition of complicated scenes. Many applications have emerged in science and in industry, ranging from 3D model acquisition, to motion capture and high performance metrology. This is due to it's versatility from high accuracy to high speed, in some cases reaching real-time performance [20]. Most structured light methods however rely on the assumption of Lambertian (diffusely reflecting) surfaces and only direct illumination. This means that global lighting effects such as intra-reflections, translucency and subsurface scattering disrupts structured light based surface scanning, causing biased, noisy or missing data.

Human and animal tissue is interesting in a number of structured light applications, including head tracking for medical motion correction [16], to robotic handling of meat in industrial settings. Each tissue type exhibits different reflection and scattering properties that can potentially disrupt a structured light scan. This paper documents the degree to which subsurface effects alter the accuracy of structured light scans in three biological tissue types; pork muscle, pork skin and pork fat. We show, that the scan error consists in part of a large deterministic part, which can be removed by means of a simple statistical error model.

2 Structured Light 3D Scanning

The structured light principle uses a calibrated camera-projector pair to identify feature correspondences and triangulate surface points, see figure 1. A large number of encoding strategies exist (see [5, 6, 18] for recent reviews). Most current high-accuracy methods are either based on binary coding schemes such as Gray codes [17] or based on sinusoidal patterns in so-called "phase shifting" [19], with many alterations

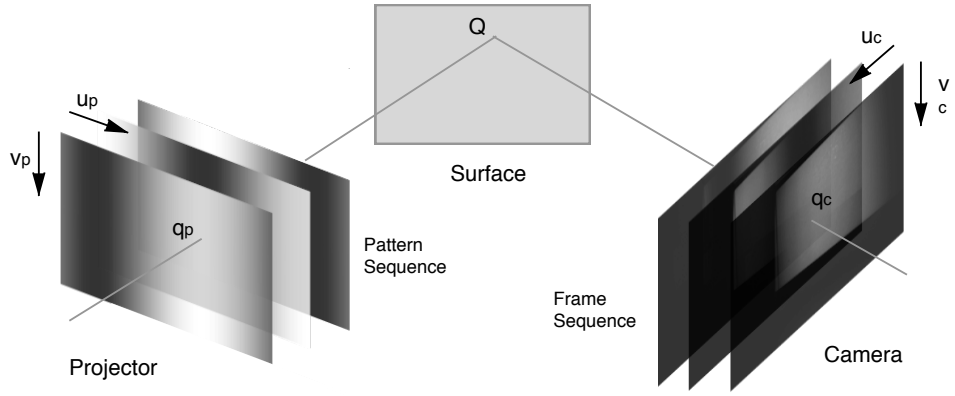

Figure 1: The structured light principle: a number of patterns are projected onto the scene, and images are captured by a camera. Correspondences are determined by different encoding algorithms, and used to triangulate points on the object surface. In this example, 3-step phase shifting patterns are shown.

and improvements to increase their accuracy, robustness or speed. Owing to the epipolar constraint in a calibrated projector-camera pair, encoding needs only to be done along one spatial direction (close to parallel to epipolar lines). With a pattern budget of N patterns, binary methods can uniquely encode 2^N lines. Phase shifting methods use at least $N = 3$ to fully encode the scene at every camera pixel. Additional patterns are used to increase the SNR, most often by projecting multiple phases of a sinusoid, and additional patterns to disambiguate between these phases in "temporal phase unwrapping". Binary coding methods are considered robust against many unwanted illumination effects, but do not make very efficient use of the pattern budget, and also fail once light stripes become too narrow. Phase shifting methods make efficient use of patterns, but provide no general means of identifying encoding errors, possibly leading to noise or outliers.

3 Global lighting effects

Under ideal circumstances, objects to be scanned with structured light exhibit only direct reflection on the object surface. Also, in order to not introduce under or over-saturation or bias in feature detection, the surface reflectance ideally is high, and Lambertian, i.e. diffusely reflecting into all directions. Under real conditions, most interesting objects exhibit global lighting effects, that is light does not reach the camera after a single scattering event on the object surface, but does so after reflecting from a distant scene point or is scattered below the surface (so-called sub surface scattering).

While some solutions have been proposed to mitigate subsurface scattering, defocus and global illumination effects [1, 2, 7], such effects are still considered harmful, and many object surfaces need to be treated by spraying them with "dulling spray" in order to make structured light possible. An even more effective way of reducing global lighting effects is by using chalk spray, which makes surfaces highly reflective and diffuse. figure 2 shows sample images of structured light patterns projected onto our samples before and after treatment with chalk-spray.

In particular the muscle samples show large degrees of subsurface scattering, which blurs and distorts the structured light patterns.

4 Related works

The issue of global lighting effects in the context of structured light has been recognised by many authors, e.g. in the acquisition of a human face reflectance field [4]. In order to reduce these in structured light scans, polarisation has been exploited in [1]. Some recent attempts have been to design structured light encoding strategies such that they are less susceptible to global lighting effects. The underlying observation is, that with high-frequent patterns, global lighting effects can be considered constant, and independent of the actual pattern. This allows for efficient separation of the observed light intensities

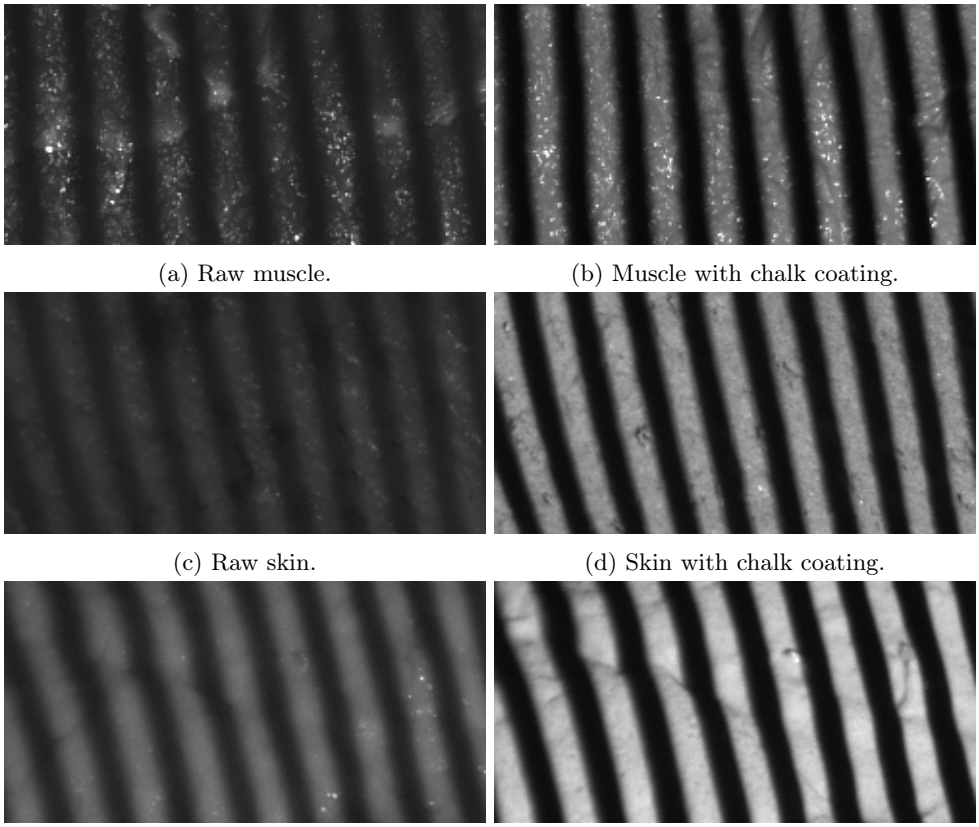

(a) Raw muscle. (b) Muscle with chalk coating.

(c) Raw skin. (d) Skin with chalk coating.

(e) Raw fat. (f) Fat with chalk coating.

Figure 2: Fine grained binary structured light pattern projected onto various types of tissues. The effect of subsurface scattering is clearly seen the pattern becomes blurred without chalk coating.

into direct and global light [15]. In modulated phase shifting [2], structured light patterns are modulated by means of carrier patterns, such that they become high-frequent in both spatial dimensions, thereby improving their separation power. Micro Phase Shifting [9] makes use of sinusoidal patterns in a narrow high-frequency band, promising robustness to global lighting effects and stable phase unwrapping with an optimal number of patterns. A newer approach is "unstructured light" [3], in which the pattern frequency can be high in both dimensions, however the number of patterns is not ideal, and the matching procedure rather cumbersome. For binary boundary methods, exclusively high or low-frequency pattern schemes can be considered robust against different global illumination effects [8].

An approach to compensate for the measurement error in isotropic semi-transparent material caused by subsurface scattering was presented in [13]. Similarly to our approach, this work empirically determines the measurement error and explains it by means of a single variable (the projected light angle), albeit only with a single verification object and structured light method. In [12], a Monte-Carlo simulation of the measurement situation was presented, which gives some insight into the error forming process.

In [10], an analytical derivation of the measurement error is given for the phase shifting methods. This error model predicts the error to decrease with increased spatial frequency of the pattern, agreeing with the theory of direct-global illumination. The model does not however take into account the loss of amplitude at higher frequency patterns, which increases noise in the measurement data.

Computer simulations of structured light scans were performed by [14] to benchmark encoding methods with respect to various parameters, and were found to have similar robustness to subsurface effects.

5 Experiments

A single camera-projector system as shown in figure 1 was used for our experiments. Surface scans were obtained from three separate tissue classes: pork muscle, pork skin and pork fat. All samples were unprocessed and not heat-treated. For each class, 8 distinct tissue samples were measured, once in their raw form, and once with chalk-spray applied. These samples were distinct placed independently in the scan volume and spanned all possible view and light angles, and also varied in their distance to the projector from approximately 200 mm to 400 mm. See figure 4 for an illustration of these parameters. The latter measurements served as a reference for the evaluation of measurement error. While we cannot assume the chalk-prepared surfaces to be noise-free, we consider them the gold-standard as they provide very clear contrast, and virtually no subsurface effects are visible (see figure 2).

In order to verify that this procedure does not alter surface geometry, we applied two separate layers of chalk to a sample object, and compared the scan result after each layer. The mean signed distance was 0.037 mm, indicating that chalk spraying the surfaces does not bias the result.

We analyse four different structured light methods, and use 12 patterns in each:

- Binary Gray coding [17]: one completely lit and one completely dark image were used to define the binary threshold individually in each camera pixel. The remaining patterns were used to encode $2^{10} = 1024$ individual lines on the object surface.
- N-step phase shifting was used with 9 shifts of a high-frequency sinusoid of frequency $1/76\,\mathrm{px}^{-1}$, corresponding to approximately 1/10 mm on the object surface. Three additional patterns were used for phase-unwrapping [11].
- Micro phase shifting [9] using the frequency vector

  $$[1/75.02, 1/70.00, 1/71.32, 1/72.47, 1/73.72, 1/76.23, 1/77.35, 1/78.40, 1/79.22, 1/80.00]\,\mathrm{px}^{-1}$$

  These frequencies corresponds to a spatial frequency on the object surface of approximately 1/10 mm. Slightly different from [9], the specific values were determined using a derivative free non-linear pattern search.
- Modulated phase shifting [2] with three shifts of a sinusoid of frequency $1/76\,\mathrm{px}^{-1}$ (1/10 mm on the object surface). Each of these sinusoids was modulated in the orthogonal direction using a sinusoidal carrier with the same frequency. Three additional patterns were used for phase-unwrapping.

Figure 3 shows the pattern sequences used in our experiments.

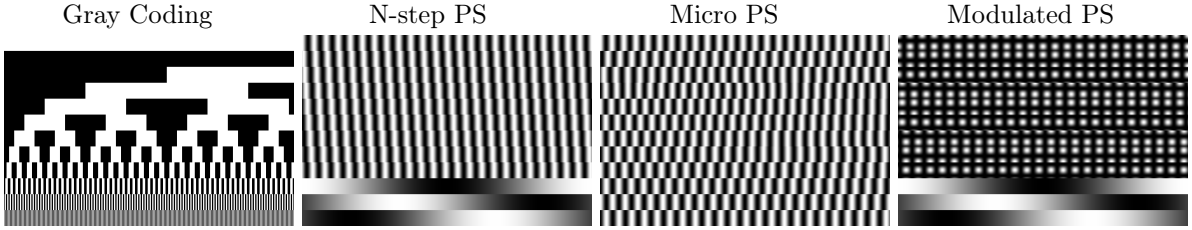

Figure 3: Structured light patterns used in our experiments. In each case, 12 patterns were used.

While binary Gray coding and N-step phase shifting can be considered well-established "reference" methods, the other two phase shifting based methods are state-of-the-art and specifically designed to mitigate subsurface effects. For every sample, we defined a binary mask within which all possible surface points were reconstructed. This ensured that the exact same surface region was used in the evaluation of each method.

Analysis consisted in determining the error in each surface point, by determining its' signed distance to the corresponding point in the chalk-sprayed reference. For Gray-code measurement, we determine the point-to-surface distance as given in the following,

$$s_j = \min_i \left[\boldsymbol{n_i} \cdot (\boldsymbol{p_j} - \boldsymbol{p_i}) \right], \tag{1}$$

where,

$\boldsymbol{p_j}$ is the jth point in the raw point cloud,
$\boldsymbol{p_i}$ is the ith point in the reference point cloud,
$\boldsymbol{n_i}$ is the ith normal in the reference point cloud,
s_j is the signed error at jth data point.

So for each a point we find its' nearest neighbour in the reference cloud in terms of normal distances. This is done as the reconstructed points are not defined in the regular camera pixel grid. As this is the case with the other methods we can simply match points using their position in the pixel grid.

5.1 Error Model

Our principle assumption is that the error is composed of a deterministic part, which once determined can be subtracted from future scans, in order to improve the accuracy. Previous work gives some hints as to which parameters to include [10,13]. Considering the scan setup, as shown in figure 4, we include three variables in our error model: the view angle (relative to the surface normal) θ_{view}, the light angle θ_{light}, and the distance from projector to object, d. We have tried to include many other variables, including reflected light to view angle and coding direction normal vector angles. These variables are inspired by the analytical error model of [10], but did not explain sufficient variance to include them in our model.

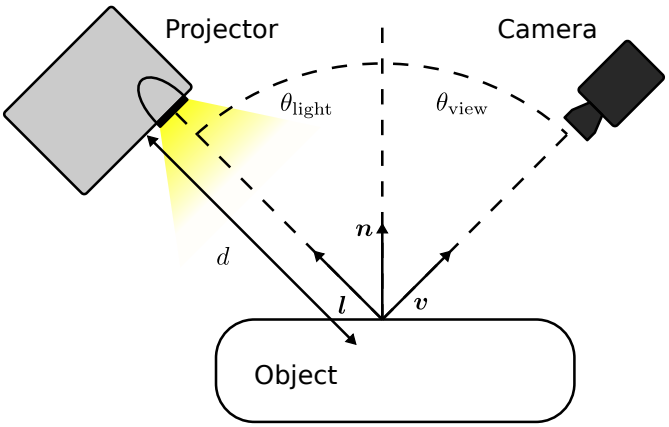

Figure 4: The structured light scanning setup with the parameters of our error model. The surface normal is $\boldsymbol{n}$, view direction $\boldsymbol{v}$, light direction $\boldsymbol{l}$ and the projector-surface distance is d.

We construct the following linear model:

$$y = \beta_0 + \beta_1 \cdot \theta_{\text{view}} + \beta_2 \cdot \theta_{\text{light}} + \beta_3 \cdot d \quad ,$$

for each of the tissue types, and fit it to a training set consisting of 90% of all observations. A test set composed of the remaining 10% was then corrected using the predetermined model.

6 Results

The parameters obtained after fitting the error model to our data are seen in tables 1, 2, and 3. These tables also show the mean signed distance before applying the model, $\epsilon_{\text{training}}$. After applying the linear model, the mean of residuals naturally is zero. We also show the standard deviation of errors before correction using the model, σ_{training}, and after, $\sigma_{\text{corrected}}$.

Figures 5, 6 and 7 show the signed error on a single sample visually before and after applying the correction model. We see qualitatively in the signed errors of Figures 5 – 7, that a clear positive bias is present in all scans (the raw surface is observed further away from the camera). This effect is especially pronounced in the muscle and skin tissue classes and with the N-step phase shifting method (this is a general observation in all muscle and skin samples). Tables 1 and 2 show that the observed bias is

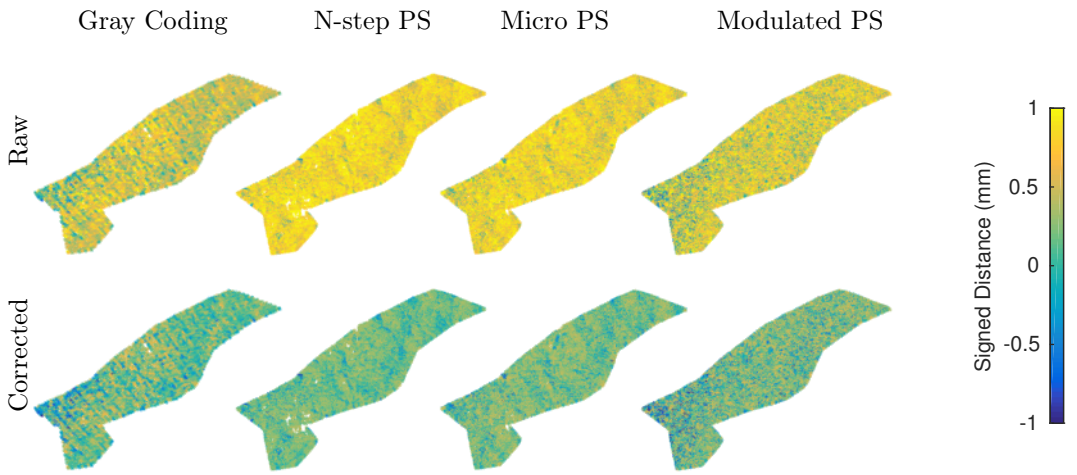

Figure 5: Signed distance (sd) between scan and reference on a single sample of muscle. Top row: before applying the linear correction model. Bottom row: after correction.

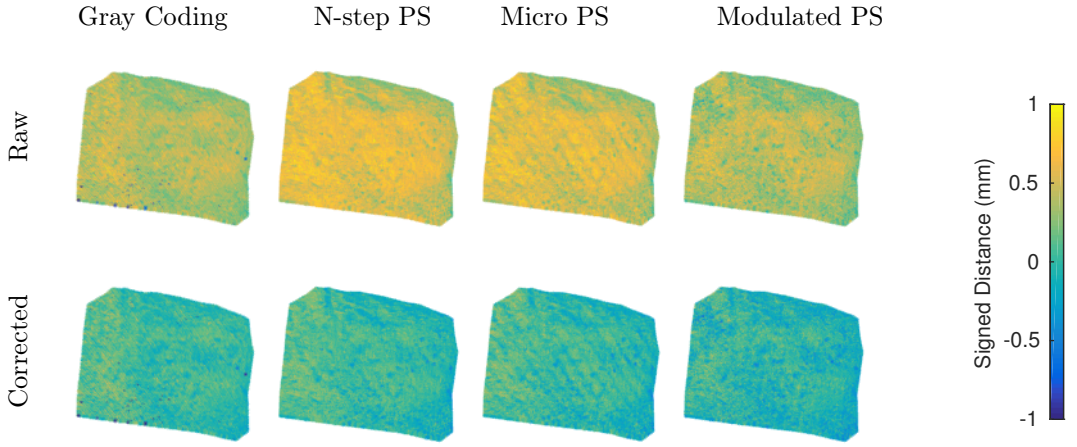

Figure 6: Signed distance (sd) between scan and reference on a single sample of fat. Top row: before applying the linear correction model. Bottom row: after correction.

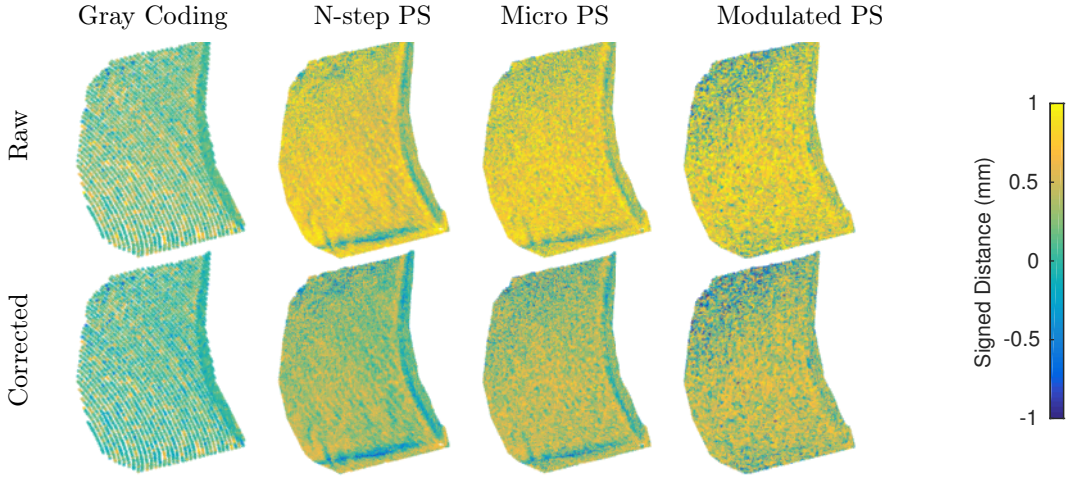

Figure 7: Signed distance (sd) between scan and reference on a single sample of skin. Top row: before applying the linear correction model. Bottom row: after correction.

	Gray Coding	N-step PS	Micro PS	Modulated PS
Intercept	0.25	0.55	0.45	0.39
θ_{view}	-0.064	-0.21	-0.15	-0.0032
θ_{light}	0.03	0.053	0.025	-0.048
d	0.00023	3.9×10^{-5}	5.1×10^{-5}	-7.1×10^{-5}
$\epsilon_{\text{training}}$	0.32	0.45	0.38	0.33
σ_{training}	0.27	0.22	0.23	0.27
$\epsilon_{\text{corrected}}$	-0.00097	-0.00094	0.0006	-0.0014
$\sigma_{\text{corrected}}$	0.27	0.22	0.23	0.26

Table 1: Estimated parameters for the linear correction model for muscle and the mean bias ϵ and standard deviation σ of the training set and the corrected test data set. The number of training samples was $N_{\text{training}} = 1\,122\,534$ and the number of test samples $N_{\text{training}} = 124\,726$.

	Gray Coding	N-step PS	Micro PS	Modulated PS
Intercept	0.038	0.89	1.00	0.76
θ_{view}	-0.0026	-0.15	-0.15	-0.06
θ_{light}	-0.24	-0.14	-0.12	-0.14
d	0.0013	-0.00062	-0.0011	-0.00068
$\epsilon_{\text{training}}$	0.35	0.51	0.48	0.41
σ_{training}	0.19	0.19	0.2	0.22
$\epsilon_{\text{corrected}}$	0.00039	-3.7×10^{-5}	-0.00045	0.00078
$\sigma_{\text{corrected}}$	0.19	0.18	0.19	0.22

Table 2: Estimated parameters for the linear correction model for skin and the mean bias ϵ and standard deviation σ of the training set and the corrected test data set. The number of training samples was $N_{\text{training}} = 3\,603\,495$ and the number of test samples $N_{\text{training}} = 400\,388$.

	Gray Coding	N-step PS	Micro PS	Modulated PS
Intercept	0.082	0.041	0.04	0.07
θ_{view}	-0.083	-0.19	-0.12	-0.081
θ_{light}	-0.019	0.092	0.041	0.026
d	0.00018	0.00037	0.00028	0.00014
$\epsilon_{\text{training}}$	0.087	0.14	0.11	0.097
σ_{training}	0.25	0.16	0.16	0.17
$\epsilon_{\text{corrected}}$	0.00075	0.00037	5.1×10^{-5}	-0.00046
$\sigma_{\text{corrected}}$	0.24	0.16	0.16	0.17

Table 3: Estimated parameters for the linear correction model for fat and the mean bias ϵ and standard deviation σ of the training set and the corrected test data set. The number of training samples was $N_{\text{training}} = 1\,868\,574$ and the number of test samples $N_{\text{training}} = 207\,619$.

around 0.6 mm for phase shifting based methods in muscle and skin, while it is only 0.32 mm for Gray coding. The same superiority of Gray coding is observed in the fat tissue class, albeit with generally much lower numbers. This is presumably due to the fact that fat appears more optically dense (see figure 2).

While some spatial structure is visible in the bias seen on Figures 5 – 7, the included variables, θ_{view}, θ_{light}, d, did only explain a small part of the variance. Hence, $\epsilon_{\text{corrected}}$ is reduced significantly from $\epsilon_{\text{training}}$, while that is not the case with $\sigma_{\text{corrected}}$ and σ_{training}.

7 Conclusion

In this work, we performed structured light scans of biological tissue, pork muscle, pork skin and pork fat, with a selection of reference and modern structured light methods. We used a linear error model to describe measurement error, and found it to be composed of a significant bias (≈ 0.5 mm for muscle, ≈ 0.3 mm for skin, and ≈ 0.1 mm for fat), which can be corrected easily. This methodology allowed us to improve the accuracy of structured light scans, given the specific tissue type. The error correction

method proposed is applicable to any type of homogenous material. While the linear parameters need to be determined beforehand, and vary widely between materials, many applications do involve only homogenous material with uniform optical properties. We also undertook an analysis of the impact of illumination spectrum on scanner accuracy. We found that blue light in general outperforms green and red when 3D scanning biological tissue.

As such, we consider our finding interesting information on the accuracy that can be obtained with structured light in general, and our methodology to apply in many common scenarios.

References

[1] Tongbo Chen, Hendrik P A Lensch, Christian Fuchs, and Hans Peter Seidel. Polarization and phase-shifting for 3D scanning of translucent objects. *Proc. IEEE CVPR*, 2007.

[2] Tongbo Chen, Hans-Peter Seidel, and Hendrik P.A. Lensch. Modulated phase-shifting for 3D scanning. *Proc. IEEE CVPR*, pages 1–8, 2008.

[3] Vincent Couture, Nicolas Martin, and Sébastien Roy. Unstructured light scanning robust to indirect illumination and depth discontinuities. *Int. Journal on Computer Vision*, 108(3):204–221, 2014.

[4] Paul Debevec, Tim Hawkins, Chris Tchou, Haarm-Pieter Duiker, Westley Sarokin, and Mark Sagar. Acquiring the reflectance field of a human face. *Proc. SIGGRAPH*, pages 145–156, 2000.

[5] Jason Geng. Structured-light 3D surface imaging: a tutorial. *Advances in Optics and Photonics*, 160(2):128–160, 2011.

[6] Sai Siva Gorthi and Pramod Rastogi. Fringe projection techniques: Whither we are? *Optics and Lasers in Engineering*, 48(2):133–140, 2010.

[7] Mohit Gupta, Amit Agrawal, Ashok Veeraraghavan, and Srinivasa G. Narasimhan. Structured light 3D scanning in the presence of global illumination. *Proc. IEEE CVPR*, pages 713–720, jun 2011.

[8] Mohit Gupta, Amit Agrawal, Ashok Veeraraghavan, and Srinivasa G. Narasimhan. A Practical Approach to 3D Scanning in the Presence of Interreflections, Subsurface Scattering and Defocus. *Int. Journal on Computer Vision*, 102(1-3):33–55, aug 2012.

[9] Mohit Gupta and Shree K Nayar. Micro Phase Shifting. *Proc. IEEE CVPR*, pages 813–820, 2012.

[10] Michael Holroyd and Jason Lawrence. An Analysis of Using High-Frequency Sinusoidal Illumination to Measure the 3D Shape of Translucent Objects. *Proc. IEEE CVPR*, pages 2985–2991, 2011.

[11] J M Huntley and H Saldner. Temporal phase-unwrapping algorithm for automated interferogram analysis. *Applied Optics*, 32(17):3047–3052, 1993.

[12] Peter Lutzke, Stefan Heist, Peter Kühmstedt, Richard Kowarschik, and Gunther Notni. Monte Carlo simulation of three-dimensional measurements of translucent objects. *Optical Engineering*, 54(8):084111, 2015.

[13] Peter Lutzke, Peter Kühmstedt, and Gunther Notni. Measuring error compensation on three-dimensional scans of translucent objects. *Optical Engineering*, 50(6):063601, 2011.

[14] Esdras Medeiros, Harish Doraiswamy, Matthew Berger, and Claudio T Silva. Using Physically Based Rendering to Benchmark Structured Light Scanners. *Pacific Graphics*, 33(7), 2014.

[15] Shree K. Nayar, Gurunandan Krishnan, Michael D. Grossberg, and Ramesh Raskar. Fast separation of direct and global components of a scene using high frequency illumination. *ACM Trans. on Graphics*, 25(3):935, 2006.

[16] Oline Vinter Olesen, Rasmus R. Paulsen, Liselotte Højgaard, Bjarne Roed, and Rasmus Larsen. Motion tracking for medical imaging: a nonvisible structured light tracking approach. *IEEE Trans. Medical Imaging*, 31(1):79–87, jan 2012.

[17] J.L Posdamer and M.D Altschuler. Surface measurement by space-encoded projected beam systems. *Computer Graphics and Image Processing*, 18:1–17, 1982.

[18] Joaquim Salvi, Sergio Fernandez, Tomislav Pribanic, and Xavier Llado. A state of the art in structured light patterns for surface profilometry. *Pattern Recognition*, 43(8):2666–2680, 2010.

[19] V Srinivasan, H C Liu, and M Halioua. Automated phase-measuring profilometry: a phase mapping approach. *Applied Optics*, 24(2):185, 1985.

[20] Jakob Wilm, Oline V. Olesen, and Rasmus Larsen. SLStudio : Open-Source Framework for Real-Time Structured Light. *Proc. IPTA 2014*, 2014.